# An analysis of the use of hyperspectral data for roundwood tracking [*]

Georg Wimmer[1][0000−0001−5529−0154], Rudolf Schraml[1], Heinz Hofbauer[1],
Alexander Petutschnigg[2], and Andreas Uhl[1]

[1] University of Salzburg, Jakob-Haringer-Strasse 2, 5020 Salzburg, Austria,
`{gwimmer,hofbauer,uhl}@cs.sbg.ac.at, rudolf.schraml@sbg.ac.at`
[2] University of Applied Sciences Salzburg, Markt 136a, 5431 Kuchl, Austria
`alexander.petutschnigg@fh-salzburg.ac.at`

**Abstract.** Traceability of round wood from the forest to the industry is a crucial issue to secure sustainable material usage as well as to optimize and control processes over the whole supply chain. There are previous works on individual wood log tracing but there is no systematic and complete technology to track individual logs from the forest to the industry. In this work we analyze if it is beneficial to employ hyperspectral image data from log ends instead of image data from standard RGB cameras. First, we compare the hyperspectral log image data across the spectral range using various well known image descriptors. In that way we analyze differences in the image data across the spectral range and find out which spectral ranges are best suited for log tracking. In a further step we present a novel approach to combine information across different spectra in order to gain valuable additional information on the annual ring pattern, the most important feature for log tracking.
We will show that there are clear differences of the log images at different spectra and that our proposed approach to combine the information of log images at different spectra provides a clearly better visibility of the annual ring pattern than single spectral images and also common RGB images.

**Keywords:** Roundwood tracking · Hyperspectral Imaging

## 1 Introduction

Traceability of roundwood from the forest to further processing companies is a recent topic of research, as customers are getting more interested in the origin of their products. This led to certificates like the one of the Forest Stewardship Council [9] or the program for the Endorsement of Forest Certification [14] that are documenting the sustainable production of wood. Even more legal actions and agreements like the European timber regulation EUTR No. 995 2010 [7] were developed. This was done to claim disclosure of the provenance of timber

---

and timber products that are placed on the European market in order to stop illegal deforestation and trading of timber.

This topic is in the view of recent research all over the world and even scientific hackathons are organized (e.g. the Evergreen innovation camp 2019 in Vienna [8]) to solve the question of traceability of wood from the forest to the related industry. Common methods for log tracing are the application of barcodes and the usage of radio frequency identification (RFID) transponders (e.g. [22] or [1]). However, these tracking systems are only used for relatively high priced lumber up to now since they require physical markings of each tree which is expensive. An alternative to physical marking is to use biometric characteristics from log images to recognize each individual log as shown in [21, 19, 17, 20, 23, 24]. The usage of log image characteristics for tracking logs is not a new idea. E.g. in [5] and [6], surface properties of wood logs were used for identification.

Hyperspectral images contain not only the visible spectra, but depending on the technology also parts of the ultraviolet (UV)-spectra and near infrared (NIR) spectra. Hence, this imaging technology has good chances to improve wood log tracking compared to common RGB images. The usage of hyperspectral imaging technologies ranges from large scale imaging down to lab scale sensors used in food safety, pharmaceutical applications forensic etc. (examples are shown in [2] or [15] ) and therefore is very common in use. Hyperspectral images have already been employed to determine the transition between juvenile and mature wood [16] and to predict the moisture content of wood [4]. In [18], hyperspectral log images were analyzed for the use of log tracking. Using an approach developed for fingerprint tracking based on Gabor filters, hyperspectral images of logs at different spectra were compared in order to find out which spectra contain the same or different information than other spectra. This knowledge can be used to reduce the technical efforts and expenses for the collection of log image data and to improve image acquisition.

So, in [18] one concrete method was employed to compare the images at different spectra. In this work we employ several well known methods, all analyzing different image properties, to compare log images at different spectra. In that way we aim to find out what are the specific differences of images at different spectra.

The annual ring pattern is arguably the most important feature for log tracking using log end images, since it provides information about the shape of the tree cross section over the entire lifespan of the tree (the annual rings) and also the growth of the tree per year (annual ring thickness). Other features like wood coloration, knots and the saw cut pattern that are visible in the log cross section may totally change if a log is capped. Therefore, we run experiments to compare the visibility of the annual ring pattern between spectral log images and common RGB log images to find out if hyperspectral images are really better suited for log tracking than common RGB images.

So far no attempt has been made to combine information on log images across different spectra. In this work, we propose an approach to construct a new log

(a) Scanning system

(b) Wood disc storage

(c) Hyperspectral cube cropping

**Fig. 1.** The sensor system shows the line scanner which was mounted on a metal frame and the slice is moved perpendicular to the scanned line manually. The stored samples were closed airtight to avoid surface changes. Each hyperspectral cube was cropped to reduce the massive amount of data.

image by combining the information on the annual ring pattern from images of the same log at different spectra.

## 2 Materials

### 2.1 Wood samples

Initially, 100 different Norway (*Picea Abies*) spruce logs (4.5 m length) were collected. For the experiments in this paper, a wood disc was cut from the lower end of each log. The outside of each disc was sanded to reduce the influence of manual chainsaw cuts at scanning. To avoid surface cracks due to wood shrinkage and discoloration due to oxidation processes, the slices were packed individually in plastic bags during transport and intermediate storage.

### 2.2 Scanning system

The samples were scanned using a FX17 multispectral line scanner, which provides scans between 990nm to 1665nm with a bandwidth of approx. 3 nm. The Specim FX17 uses mainly parts of the NIR spectra. For the scanning setup a resolution of 640x640 pixel was chosen. The scanning system is shown in Fig. 1. Halogen light was used for lighting. Each disc was pushed through the system by hand and the speed was synchronized with a trigger. The hyperspectral data, i.e. the translation from line scanning data to a hyperspectral cube, was performed by the acquisition software Perception Studio. For each hyperspectral cube the grayscale images (PNG) for each band were extracted and show the cross section (CS) of the disc. This results in 196 images per wood disc. This conversion enables to apply standard image processing algorithms. From 13 discs, image data was lost during acquisition and so hyperspectral data is only available from 87 discs. Unfortunately, the obtained spectral images from the FX17 scanner are a
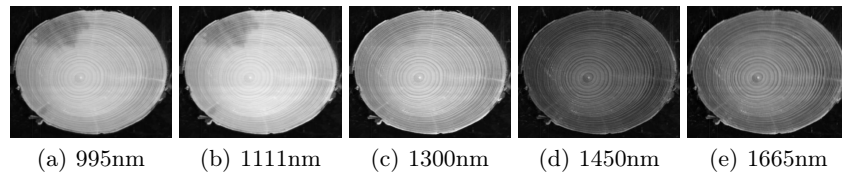
<div align="center">

(a) 995nm     (b) 1111nm     (c) 1300nm     (d) 1450nm     (e) 1665nm

</div>

**Fig. 2.** Images of the same disc at different spectra.



<div align="center">

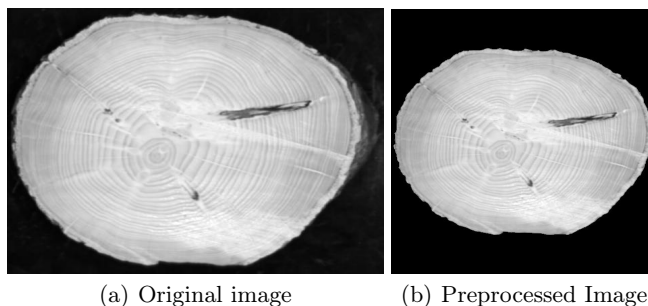(a) Original image          (b) Preprocessed Image

</div>

**Fig. 3.** An example of an original image and its segmented, quadratic output after preprocessing the image.

bit squeezed in height. This can be observed by comparing the spectral images with the RGB image of the same log in Fig. 6. We assume that this is caused by the acquisition software and an inaccurate trigger synchronization.

Exemplar images of one log at 5 different spectra are shown in Fig. 2. As we can observe, the images at different spectra have clearly different brightness distributions and also the contrast is different. The spectral image at 1111nm is clearly the brightest and the image at 1450nm is clearly the darkest one, so there is no constant change in one direction regarding the brightness of the images along the spectral range.

Additionally, RGB images were taken from all 100 discs using a Canon 70D camera. The camera has been fixed so that the images were all taken under the same viewpoint and the same scale. In our experiments to compare RGB and spectral image data, we employ one RGB image from each of the 87 discs for which hyperspectral data is available. An example of an RGB image together with examples of spectral images from the same disc can be observed in Fig. 6.

### 2.3   Image segmentation

The spectral images are rather easy to segment since they have a nearly black background outside of the CS. Like in a previous publication on log tracing [24], we apply the active contour method [3] for the segmentation of the log images. The image is reduced to the smallest possible box shaped size so that the log is still fully included in the image and those parts of the image that have been found

to be part of the background are set to black. To be able to extract information from the images using a variety of different feature extraction methods and to be able to compare the extracted features of different images, we decided to turn the box shaped segmented images into squares of equal size for all log images. This is done by making the images quadratic by padding the images with black background on the smaller side of the box shaped image so that the log is centered in the now quadratic image. Then a five pixel thick black border is added on each side of the image and the images are resized to the size of $352 \times 352$. In Fig. 3 we can see an example of an original image and its quadratic segmented output. All experiments are applied to these preprocessed images.

The 87 RGB images are processed in the same way as the spectral images with the only difference that the segmentation is applied using CNNs (see [23]).

## 3   Methods

### 3.1   Differences of spectral images along the spectral range

In this work we employ various feature extraction methods that analyze different features of the spectral images along the spectral range. We employ image histograms that analyze the brightness distribution of the images, features extracted by CNNs, an LBP method that basically compares the brightness between pixels and their neighbored pixels, and the Gabor wavelet transform, that analyzes the frequency distribution of images along different directions. For all these methods, feature vectors are computed for each image of a log end along the spectral range. Distances between feature vectors of a log at different spectra are computed using the Euclidean distance.

Additionally to the feature extraction methods we compute the average pixel difference between images at different spectra. We further denote this method as 'Image Difference' or 'ImDiff'. Furthermore, we apply the edge metric LEG that analyzes changes in the edge information between images.

**Image Histogram:** Histograms of the images are build where the number of pixels for each pixels brightness value between 0 and 255 is counted. So the resulting histogram of an image has 256 bins.

**CNN Transfer Learning:** For CNN feature extraction, we use a DenseNet161 [11] convolutional neural network (CNN) that has been trained on the ImageNet database. As features we extract the CNN activations of an intermediate layer by simply removing the final layer of the CNN. The log images are normalized and resized to the size of $224 \times 224$ and then fed to the CNN resulting in 2208 dimensional feature vectors.

**LBP:** Based on a grayscale image, the LBP operator generates a binary sequence for each pixel by thresholding the neighbors of the pixel by the center pixel value. The binary sequences are then treated as numbers (i.e. the LBP numbers). Once all LBP numbers for an image are computed, a histogram based on these numbers is generated and used as feature vector. We employ the multiscale block binary patterns (MB-LBP) operator [13] with three different block

sizes (3,9,15). The uniform LBP histograms of the 3 scales (block sizes) are concatenated resulting in a feature vector with $3 \times 59 = 177$ features per image.

**Gabor Wavelets:** The Gabor Wavelets transform (GWT) [12] is a multi-scale and multi-orientation wavelet transform that decomposes an image in subbands that contain information at different frequency bands (scales) and orientations of an image. The GWT is applied using 3 decomposition levels and 6 orientations. The feature vector of an image consists of the statistical features mean and standard deviation of the absolute values of the subband coefficients from each of the 18 (3x6) subbands.

**Local Edge Gradients (LEG)** The LEG [10] analyses changes in the edge information between two images. LEG combines the edge change, based on the local binary pattern concept, and the edge gradient change. The edge change is calculated in the low frequency band and the gradient change in the high frequency band of a wavelet decomposition of the images. The LEG is a quality metric, a high metric score reflects a high similarity between two images, with a normalized score in $[0, 1]$.

### 3.2    Combination of spectral images

The most important feature to trace logs is the annual ring pattern. In [24], a filtering approach was proposed for log end images that highlights the annual ring pattern and widely ignores all other features of the image. Using this filtering approach as preprocessing for a CNN-based log recognition clearly improved the results for the difficult scenario of log tracing from the forest to the sawmill using image data acquired from totally different sources (see [24]). The images were first recorded using a Canon 70D camera (the RGB data that is also used in this work) and later at the sawmill using a CT scanner.

The advantage of the filtering approach is that the filter response images offer a very good visibility of the annual ring pattern but mostly ignore features that are problematic for wood log tracing like knots that either completely change or even disappear or reappear in the log cross section after the log is capped, which is regularly done at sawmills before processing the log.

The filtering approach [24] is applied using directional Gaussian 2D filters at 8 different directions (0°, 22.5°, 45°, . . . 157.5°). The filters are shown in Fig. 4 on the left side. To specifically highlight the annual ring pattern, the direction of the filters has to be similar to the direction of the annual year rings at each position of the log. This is ensured by subdividing the log into 16 different sectors, where each sector covers the part of the log within a range of 22.5° using the pith as center point. Then each sector is filtered separately with the filter that has the same direction as the annual year rings in the respective sector (see Fig. 4, right side). To ensure that mainly filter responses of the annual ring pattern remain, all filter response values that are smaller than zero are set to zero. For a better visibility of the annual ring pattern, the brightness values are normalized so that the maximum brightness value of a filter response image is 255 and the minimum is 0, followed by the application of adaptive histogram equalization. For more details on the filtering process see [24]. In Fig. 6 (a-c), we can observe spectral
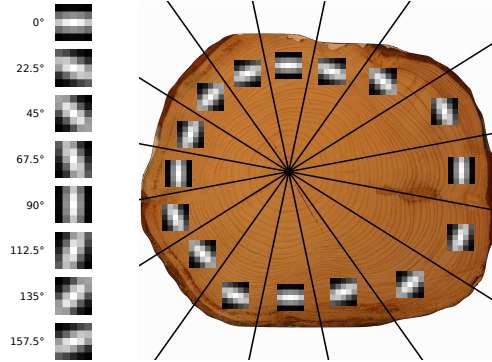
**Fig. 4.** Division of the log in 16 sectors and the associated filters for each sector.

images (top row) and their corresponding filter responses (middle row).

A further advantage of the filter response images compared to the original spectral images is that the information on the annual ring pattern of a log across different spectra can be combined in a simple way. Our proposed approach constructs an image from the filter response images of the 196 spectral images of a log by taking the maximum pixel brightness value across the 196 filter resposes at each pixel position.

This is possible because the log cross section is always positioned exactly the same for the 196 spectral images of one log. We denote this approach as Maximum Filter approach (MF). Some of the annual rings are only clearly visible under certain spectra and by taking the maximum filter response of all images along the spectral range for each pixel position separately, we aim to gain the best possible visibility of the annual ring pattern for the MF image among the spectral images at each position of the log. In Fig. 6 (d) in the middle row we show an example of an MF image along with three of the 196 spectral images (Fig. 6 (a-c)) from which it was constructed.

Now we need a way to be able to quantify the visibility of the annual ring pattern and to compare it between the spectral images, MF images and RGB images. For this, we first binarize the filter response images and the MF image using adaptive thresholding by calculating locally adaptive image thresholds which are chosen using local first-order image statistics around each pixel (using the Matlab function "imbinarize(I, 'adaptive')"). Then, skeletonization is applied to the binarized filter response images. To remove noise and components that are too small to properly indicate the annual rings, all connected components that have less than 20 pixels are removed from the skeletonized images. Examples of skeletonized filter response images can be seen in Fig. 6 in the bottom row. Now by counting the white pixels in the skeletonized images (which indicate annual rings), we get an estimation of the visibility of the annual ring pattern in the filter response images and the original images itself. The higher the number of white pixels, the better the visibility of the annual ring pattern.

## 4   Experimental Setup

Since we are mainly interested in the general differences between log images at different spectra and not in the differences for specific logs, we average the outcomes of the employed methods from Section 3.1, that are applied to each log separately, over all 87 logs.

In case of the methods extracting feature vectors (Image Histogram, CNN, LBP and Gabor Wavelets) we compute the Euclidean distances between the feature vectors of all 196 spectral images from each log separately. For LEG, we compute distances $d$ by inverting the metric scores $s$ between the 196 images per log ( $d = |1 - s|$ ). Hence, for each of the methods we get a distance matrix of $196 \times 196$ for each of the 87 logs. Then each of the 87 distance matrices is normalized separately by dividing all its entries by the highest occurring distance in the matrix so that the values in each matrix are exactly between 0 and 1. Finally, the 87 normalized distance matrices are averaged by taking the average value over the 87 different distance values for each position in the matrices, so that we gain the average distances between the images at different spectra over the 87 logs in the form of a $196 \times 196$ distance matrix for each of the methods.

For the method Image Difference we proceed similar, but here we are more interested in the absolute values of the differences between images and hence we do not normalize the differences for each log. Also here we get a $196 \times 196$ matrix that shows the differences between the images per log that is averaged over the 87 logs.

The two methods 'Image Difference' and 'Image histogram' are not only applied to the original spectral images but also to images that are normalized with regard to the average pixel brightness and the image contrast. Once again, the normalization is applied separately for the images of different logs, First, the mean and the standard deviation are computed for each spectral image of a log, then the average over the 196 means (M) and standard deviations (SD) is computed per log. Finally, each spectral image $I$ of a log is normalized by setting the standard deviation of the image to SD ($I = I \times SD/std(I)$) followed by setting the mean value to M ($I = I + M - mean(I)$). In that way, the normalized spectral images of one log all have the same mean brightness and at least similar contrast. So, by additionally applying the two methods to the normaized images, we can analyze the differences of log images at different spectra apart from the two factors average image brightness and contrast.

## 5   Results

In Fig. 5 (a,b) we present the results of the method Image Difference, where the mean pixel difference between images at different spectra is averaged over the 87 logs. We can observe that the differences between the normalized spectral images are about 4 times lower than the differences of the original image for all comparisons between images at different spectra. So, alone the normalization of the images eliminates about 3 quarters of the differences between images at
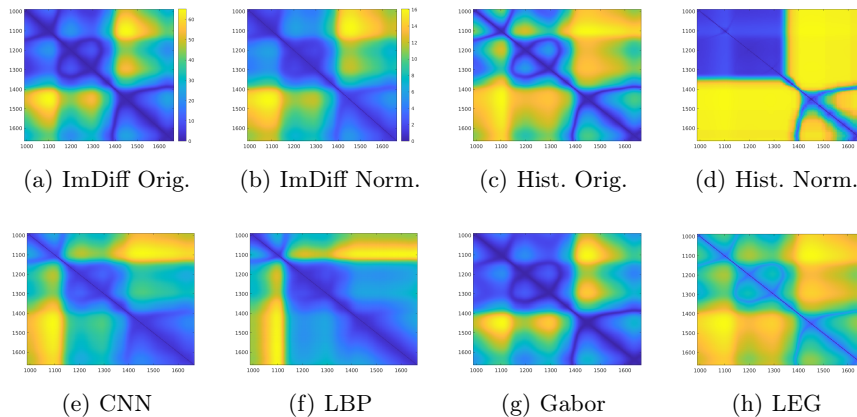
**Fig. 5.** Heatmaps showing the differences (a-b) and distances (c-h) between spectral images in the range of 990-1665, averaged over the 87 logs. The Image Difference method (a,b) and the Image Histogram method (c,d) show the differences respectively distances for original and normalized images. (e), (f), (g) and (h) show the distances for the methods CNN, LBP, Gabor Wavelets respectively LEG.

different spectra. Generally, the differences between images at spectra between 990nm and about 1350nm are rather small and the same applies for images at spectra between about 1400 and 1665nm. The highest differences are between images in the spectral range of 990-1150nm and images in the spectral range of about 1400-1600nm.

In Fig. 5 (c-h) we compare the distances between images at different spectra using 5 different methods. We can observe that for the Image Histogram method (Fig. 5 (c) and (d)), which shows the distribution of the brightness values in an image, the distances between images are quite different for original and normalized images. In case of the original images, the distances between different spectra behave similar as for the Image Difference method, but with bigger differences between images in the spectral range of 990-1150nm and images in the spectral range of 1150-1350nm. The distances between the normalized images at different spectra are totally different. Here, the distances are quite low between images in the spectral range of 990-1350nm. For nearly all other comparisons of images at different spectra, the distances are high, even for rather small differences in the spectrum (>30-50nm difference).

For the LBP method, which basically compares the brightness between pixels and their neighbored pixels, the distances are different than for the results of the previously analyzed methods. Here, the distances between images at the wide spectrum from about 1150-1665nm are rather low. The highest difference occur between images in the spectrum of 990-1130 and images at spectra higher than 1400nm. The distances between the CNN features are similar to those of the
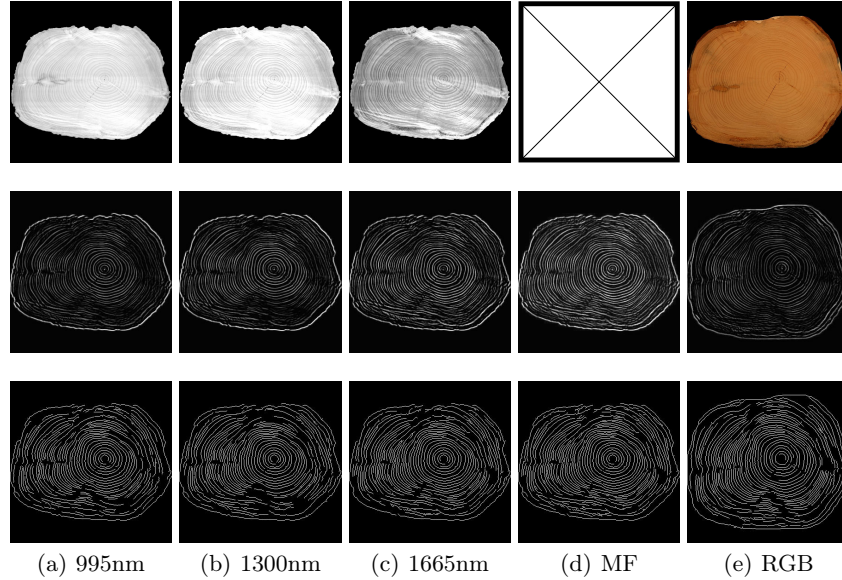
(a) 995nm          (b) 1300nm          (c) 1665nm          (d) MF          (e) RGB

**Fig. 6.** Original images (top row), filter response images (middle row) and skeletonized filter responses (bottom row) of images from the same log. The three columns on the left side (a-c) show spectral images at different spectra and their filter responses and skeletonization. The fourth column (d) shows the output of the Maximum Filter approach and its skeletonization. The right column (e) shows an RGB image and its filter response and skeletonization.

LBP approach and the Image Histogram method using the original images, kind of a mixture between the distances of the two methods.

The distances between images using Gabor Wavelets, which analyzes the frequency distribution of images along different directions, are quite similar in behaviour as for the Image Difference method.

The distances between images using LEG, which compares the edge information between images, are kind of similar to the results of the methods Image Histogram with the original images and CNN. Also the results in [18] on the differences between spectral log images from the FX17 scanner were similar to the outcomes of these three methods.

Summed up, the different methods produce different results regarding the difference of log images at different spectra, but the results of the methods are kind of similar with the exception of the method Image Histogram using normalized images. For all methods there are low distances between spectral images in the spectrum of 990-1150nm and for all methods except the Image Histogram using normalized images, the same applies to images in the spectrum of about 1150-1370nm and images in the spektrum of about 1380-1655.

In Fig. 6 we show five different images from the same log (three examples of spectral images at different spectra, the combined filter response MF and an RGB image) together with their filter response images and their skeletonization of the filter responses. When comparing the filter response images (middle row in Fig. 6) with each other, we can observe that the combined filter response image (MF) offers a better visibility of the annual ring pattern than the filter responses of images from only a single spectral image. The same can be observed for the images showing the skeletonization of the filter responses (bottom row in Fig. 6). For the shown skeletonized images, the number of white pixels indicating an annual ring is 9932 for the spectral image at 995nm, 9921 for the spectral image at 1300nm, 10528 for the spectral image at 1665nm and 11052 for MF. However, the skeletonization of the RGB image even outperforms MF with 12048 pixels. However, as can be clearly observed in Fig. 6, the cross section area of the log in the RGB image is clearly bigger than the cross section area of the spectral images. This is because the spectral images were squeezed in height during the image acquisition process (see Section 2.2) and hence their cross section areas are smaller in the square images. So that comparison is clearly not fair. A much fairer approach is to compare the percentage of white pixels in the cross section area of the log (dividing the number of white pixels by the total number of pixels in the log cross section multiplied by 100). Using this fair comparison, 15.13% of the cross section area are white pixels indicating annual ring pattern for the MF image compared to 13.78% for the RGB image, whose cross section area is about 1.197 times bigger than the cross section area of the spectral images shown in Fig. 6. So, the visibility of the annual ring pattern is actually better for the MF image than for the RGB image for the exemplar images of one log shown in Fig. 6.

In Fig. 7 we present the percentage of white pixels from the skeletonized filter responses in the cross section area. This percentage is computed for each log seperately and then the outcomes are averaged over the 87 logs. This performance measure indicates the visibility of the annual ring pattern of the log images and is presented for each of the 196 spectral images along the spectral range as well as for the MF and RGB images. Here we can clearly observe that MF offers a better visibility of the annual ring pattern than single spectral images. When we compare the spectral images with the RGB images, we can see that the spectral images only show a better visibility of the annual ring pattern in the range of about 1390nm-1490nm. MF images offer a clearly better visibility of the annual ring pattern than the filtered RGB images.

## 6    Conclusion

In this work we analyzed hyperspectral log images with respect to their application on wood log tracking. First we applied experiments to find the differences between the images at different spectra (990-1665nm). We showed that for most or even all methods there are only small differences between spectral images in the spectral ranges of 990-1150nm, 1150-1370nm and 1380-1655nm. The high-
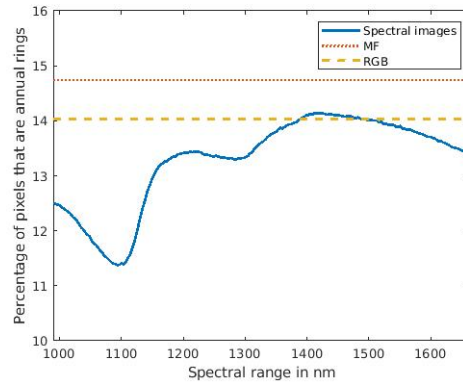
**Fig. 7.** The percentage of white pixels in the skeletonized filter responses in the cross section (CS) area averaged over all 87 logs. This performance measure indicates the visibility of the annual ring pattern and is shown for the spectral images along the spectral range as well as for the combination of spectral images (MF) and for RGB images.

est differences occured between images in the spectral range of 990-1150nm and images in the spectral range of 1400-1600nm. Second, we combined the images across the spectral range in order to maximize the image information. This was done using the proposed method MF, which combines filter response images that highlight the annual ring patter. We showed that MF offers a clearly better visibility of the annual ring pattern than single spectral images. Third, we compared the visibility of the annual ring pattern, the most important feature for log tracking, between spectral images and RGB images. We showed that only spectral images in the spectral range of about 1390nm-1490nm offer a better visibility of the annual ring pattern than RGB images of the same logs. The clearly best visibility of the annual ring pattern was achieved using MF.

## References

1. Björk, A., Erlandsson, M., Häkli, J., Jaakkola, K., Nilsson, Å., Nummila, K., Puntanen, V., Sirkka, A.: Monitoring environmental performance of the forestry supply chain using RFID. Computers in Industry **62**(8-9), 830–841 (oct 2011). https://doi.org/10.1016/j.compind.2011.08.001
2. Camps-Valls, G., Tuia, D., Gómez-Chova, L., Jiménez, S., Malo, J.: Remote Sensing Image Processing. Morgan and Claypool, San Rafael, CA (2011)
3. Chan, T., Vese, L.: Active contours without edges. IEEE Transactions on Image Processing **10**(2), 266–277 (2001)
4. Chen, J., Li, G.: Prediction of moisture content of wood using modified random frog and vis-nir hyperspectral imaging. Infrared Physics and Technology **105**, 103225 (2020). https://doi.org/https://doi.org/10.1016/j.infrared.2020.103225, `https://www.sciencedirect.com/science/article/pii/S135044951931062X`

5. Chiorescu, S., Grönlund, A.: The fingerprint approach: using data generated by a 2-axis log scanner to accomplish traceability in the sawmill's log yard. Forest Products Journal **53**, 78–86 (2003)
6. Chiorescu, S., Grönlund, A.: The fingerprint method: Using over-bark and under-bark log measurement data generated by three-dimensional log scanners in combination with radiofrequency identification tags to achieve traceability in the log yard at the sawmill. Scandinavian Journal of Forest Research **19**(4), 374–383 (2004)
7. EuropeanParliament: Regulation (eu) no 995/2010 of the European parliament and of the council of 20th October 2010 laying down the obligations of operators who place timber and timber products on the market
8. Evergreen: Homepage of the evergreen innovation camp 2019 in vienna, `www.evergreen-innovationcamp.io`
9. FSC: Homepage of the forest stewardship council, `www.fsc.org`
10. Hofbauer, H., Uhl, A.: An effective and efficient visual quality index based on local edge gradients. In: IEEE 3rd European Workshop on Visual Information Processing. p. 6pp. Paris, France (Jul 2011)
11. Huang, G., Liu, Z., Van Der Maaten, L., Weinberger, K.Q.: Densely connected convolutional networks. In: 2017 IEEE Conference on Computer Vision and Pattern Recognition (CVPR). pp. 2261–2269 (2017). https://doi.org/10.1109/CVPR.2017.243
12. Lee, T.: Image representation using 2d gabor wavelets. IEEE Transactions on Pattern Analysis and Machine Intelligence **18**(10), 959–971 (1996). https://doi.org/10.1109/34.541406, `https://www.scopus.com/inward/record.uri?eid=2-s2.0-0030259483&doi=10.1109%2f34.541406&partnerID=40&md5=8b48cbc6faf570d8427d5781261fd537`
13. Liao, S., Zhu, X., Lei, Z., Zhang, L., Li, S.Z.: Learning multi-scale block local binary patterns for face recognition. In: Advances in Biometrics. pp. 828–837. Springer Berlin Heidelberg, Berlin, Heidelberg (2007)
14. PEFC: Homepage of the programme for the endorsement of forest certification, `www.pefc.at`
15. Richards, J.A., Jia, X.: Remote Sensing Digital Image Analysis: An Introduction. Springer Verlag, New York; Berlin, Heidelberg; Germany (2006)
16. Ruano, A., Zitek, A., Hinterstoisser, B., Hermoso, E.: Nir hyperspectral imaging (nir-hi) and xrd for determination of the transition between juvenile and mature wood of pinus sylvestris l. Holzforschung **73**(7) (2019)
17. Schraml, R., Charwat-Pessler, J., Petutschnigg, A., Uhl, A.: Towards the applicability of biometric wood log traceability using digital log end images. Computers and Electronics in Agriculture **119**, 112–122 (2015). https://doi.org/10.1016/j.compag.2015.10.003
18. Schraml, R., Entacher, K., Petutschnigg, A., Young, T., Uhl, A.: Matching score models for hyperspectral range analysis to improve wood log traceability by fingerprint methods. Mathematics **8**(7), 10 (2020). https://doi.org/10.3390/math8071071, `https://www.mdpi.com/2227-7390/8/7/1071`
19. Schraml, R., Hofbauer, H., Petutschnigg, A., Uhl, A.: Tree log identification based on digital cross-section images of log ends using fingerprint and iris recognition methods. In: Proceedings of the 16th International Conference on Computer Analysis of Images and Patterns (CAIP'15). pp. 752–765. LNCS, Springer Verlag (2015). https://doi.org/10.1109/ICIP.2015.7351488

20. Schraml, R., Hofbauer, H., Petutschnigg, A., Uhl, A.: On rotational pre-alignment for tree log end identification using methods inspired by fingerprint and iris recognition. Machine Vision and Applications **27**(8), 1289–1298 (2016). https://doi.org/10.1007/s00138-016-0814-2
21. Schraml, R., Petutschnigg, A., Uhl, A.: Validation and reliability of the discriminative power of geometric wood log end features. In: Proceedings of the IEEE International Conference on Image Processing (ICIP'15) (2015). https://doi.org/10.1109/ICIP.2015.7351488
22. Tzoulis, I., Andreopoulou, Z.: Emerging traceability technologies as a tool for quality wood trade. Procedia Technology **8**, 606–611 (2013). https://doi.org/https://doi.org/10.1016/j.protcy.2013.11.087, `https://www.sciencedirect.com/science/article/pii/S2212017313001497`, 6th International Conference on Information and Communication Technologies in Agriculture, Food and Environment (HAICTA 2013)
23. Wimmer, G., Schraml, R., Hofbauer, H., Petutschnigg, A., Uhl, A.: Two-stage cnn-based wood log recognition. In: Computational Science and Its Applications – ICCSA 2021. LNCS, vol. 12955, pp. 115–125. Springer International Publishing, Cham (2021)
24. Wimmer, G., Schraml, R., Lamminger, L., Petutschnigg, A., Uhl, A.: Cross-modality wood log tracing. In: 2021 IEEE International Symposium on Multimedia (ISM). pp. 191–195 (2021). https://doi.org/10.1109/ISM52913.2021.00038